



CHORUS

This is the accepted manuscript made available via CHORUS. The article has been published as:

Cospectral budget model describes incipient sediment motion in turbulent flows

Shuolin Li and Gabriel Katul

Phys. Rev. Fluids **4**, 093801 — Published 24 September 2019

DOI: [10.1103/PhysRevFluids.4.093801](https://doi.org/10.1103/PhysRevFluids.4.093801)

1 **A co-spectral budget model describes incipient sediment motion**
2 **in turbulent flows**

3 Shuolin Li*

4 *Sibley School of Mechanical and Aerospace Engineering,*
5 *Cornell University, Ithaca, NY, USA*
6 *Nicholas School of the Environment,*
7 *Duke University, Durham, NC, USA*

8 Gabriel Katul

9 *Nicholas School of the Environment,*
10 *Duke University, Durham, NC, USA*
11 *Department of Civil and Environmental Engineering,*
12 *Duke University, Durham, NC, USA*

Abstract

13

14 Relating incipient motion of sediments to properties of turbulent flows continues to draw signif-
15 icant research attention given its relevance to a plethora of applications in ecology, sedimentary
16 geology, geomorphology, and civil engineering. Upon combining several data sources, an empirical
17 diagram between a densimetric Froude number $F_{dc} = U_c/\sqrt{gh\Delta}$ and relative roughness $N = d/h$
18 was recently reported over some 6 decades of N , where d is the grain diameter, h is the overlying
19 boundary-layer depth, U_c is the bulk velocity at which sediment motion is initiated, g is the gravi-
20 tational acceleration, $\Delta = s - 1$, and s is the specific gravity of sediments. This diagram featured 3
21 approximate scaling laws of the form $F_{dc} \sim N^{-\alpha}$ with $\alpha = 1/2$ at small N , $\alpha = 1/6$ at intermediate
22 N and $\alpha = 0$ at large N . The individual α values were piece-wisely recovered using a combination
23 of (i) scaling arguments linking bulk to local flow variables above the sediment bed and (ii) assumed
24 exponents σ for the turbulent kinetic energy spectrum $E_{tke}(k) \sim k^{-\sigma}$, where k is the wavenumber
25 or inverse eddy size. To explain the $\alpha = 1/2$, the aforementioned derivation further assumed the
26 presence of an inverse cascade in $E_{tke}(k)$ at large wavenumber (i.e. $\sigma = 3$). It is shown here that a
27 single $F_{dc} - N$ curve can be derived using a cospectral budget (CSB) model formulated just above
28 the sediment bed. For any k , the proposed CSB model includes two primary mechanisms (i) a
29 turbulent stress generation formed by the mean velocity gradient and the spectrum of the vertical
30 velocity $E_{ww}(k)$ and (ii) a destruction term formed by pressure-velocity interactions. Hence, a
31 departure from prior work is that the proposed CSB model is driven by a multi-scaled $E_{ww}(k)$
32 instead of $E_{tke}(k)$ characterized by a single exponent. Also, the CSB model does not require the
33 presence of an inverse cascade to recover an $\alpha = 1/2$. Last, the CSB approach makes it clear that
34 the scaling parameters linking local to bulk flow variables used in prior determinations of α at
35 various N must be revised to account for bed roughness effects.

* Shuolin Li: sl3259@cornell.edu

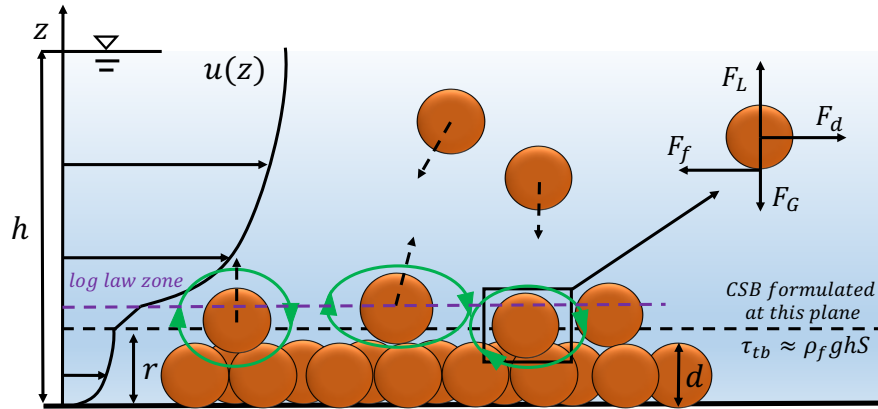


FIG. 1. Sketch of a wide rough channel whose bed is covered by spherical grain particles of uniform diameter d . The grains are entrained into the overlying turbulent flow when the surface shear stress τ_{tb} exceeds a threshold. The green arrow depicts turbulent eddies that have multiple sizes while the grains are represented by brown circles. The co-spectral budget (CSB) model is formulated in the roughness sublayer (black dashed line) above the grains but below the region characterized by a logarithmic mean velocity profile (purple dashed line). The forces acting on an individual particle are defined as follows: F_d is the drag force, F_f is the frictional force, F_G is the gravitational force related to particle weight, and F_L is the lift force.

36 I. INTRODUCTION

37 Incipient motion of grains by turbulent flows over a loose boundary continues to draw
 38 research attention in erosion studies, river bank stability, ecosystem sciences and eolian
 39 processes [1–3]. Over the course of some 100 years, such incipient motion has been described
 40 using a balance between hydrodynamic forces exerted on particles and a stabilizing force
 41 represented by the submerged particle weight as shown in Figure 1. This force-balance has
 42 been developed at the single particle scale [4] but extrapolated in space to account for multi-
 43 particle interactions using probabilistic approaches [5]. Extensions to both have also been
 44 proposed and used in a number of applications [6–8].

45 Operationally, incipient motion is described by the *Shields Diagram* [9] that empirically
 46 relates a dimensionless bed shear stress θ (labeled as the critical Shields number)

$$47 \quad \theta = \frac{u_*^2}{\Delta g d} \quad (1)$$

48 to a roughness Reynolds number Re_* using [10–12]. It is to be noted that when the shear or

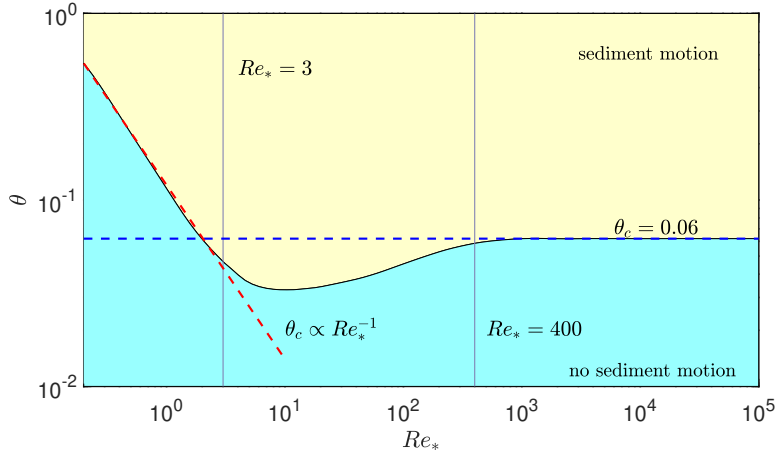


FIG. 2. Modified *Shields Diagram* fitted to the original data of Shields [9], where $\theta_c \approx 0.06$ is independent of Re_* when $Re_* > 400$ and $\theta_c \propto Re_*^{-1}$ for $Re_* < 3$. An intermediate region defined by $Re_* \in [3, 400]$ exists where $\theta_c \in [0.02, 0.06]$ varies weakly and non-monotonically with Re_* .

49 friction velocity u_* reaches the critical shear velocity u_{*c} and the sediment particle is about
50 to move, the Shields number becomes the critical Shields number θ_c . Here, the roughness
51 Reynolds number is defined as $Re_* = u_* d / \nu$, where $\Delta = s - 1 > 0$, $s = \rho_p / \rho_f$ is the specific
52 gravity of the particles, ρ_p and ρ_f are the particle and water densities respectively, g is
53 the gravitational acceleration, ν is the kinematic viscosity, $u_* = (\tau_b / \rho_f)^{1/2}$ is the friction
54 velocity, τ_b is the bed shear stress, and d is the grain diameter. Figure 2 repeats such a
55 diagram summarizing a large corpus of experiments. This diagram shows that at low Re_* ,
56 θ_c decreases with increasing Re_* , whereas θ_c becomes a constant independent of Re_* for
57 large Re_* . While the limitations of the Shields diagram have been recognized for some
58 time now [1, 13], the data presentation inspired by the Shields diagram remains popular in
59 numerous fields. Its simplicity and reasonable empirical support [14, 15] even in situations
60 that fall well outside the original domain of applicability [16–21] continue to make $\theta_c - Re_*$
61 representation attractive and a test-bed for other detailed models [22]. A case in point is
62 the use of a Shields diagram to reconstruct a number of surface features on Mars [23, 24]
63 and Titan [25].

65 An even more 'naive' but preferable approach in large-scale hydrodynamic models is to
66 use a critical bulk velocity U_c formed by a flow rate per unit cross-sectional area instead of
67 the critical shear velocity to scale particle incipient motion. This approach gained attention

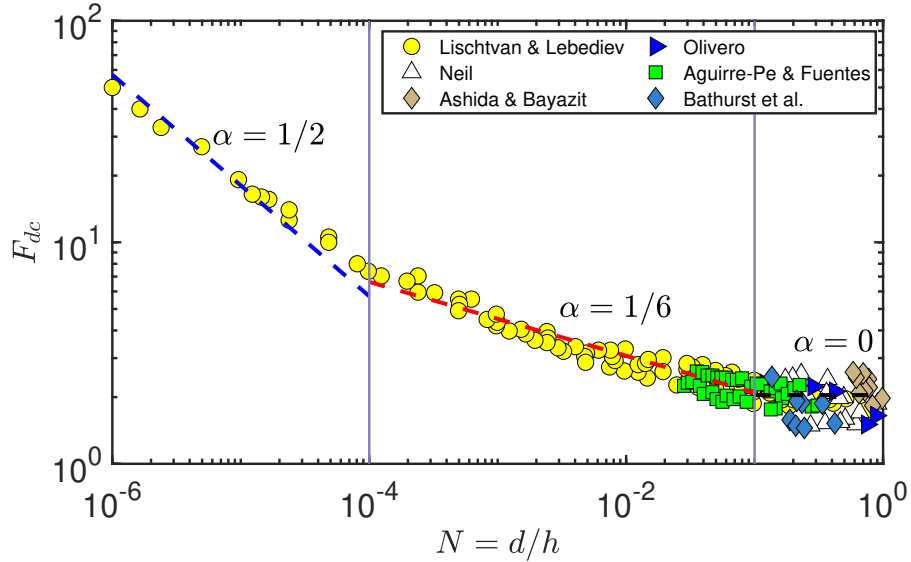


FIG. 3. The $F_{dc} - N$ diagram with data reported by Ali and Dey [3, 26] along with the three scaling laws expressed as $F_{dc} \sim N^{-\alpha}$ with $\alpha = 1/2$, $1/6$, and 0 (in dashed lines). The original data sources are described in a number of studies that include Lischtvan and Lebediev [27], Neill [28], Ashida and Bayazit [29], Olivero [30], Aguirre-Pe and Fuentes [31], Bathurst *et al.* [32, 33].

68 after Ali and Dey [3, 26] reported a remarkable link between a densimetric Froude number
69 $F_{dc} = U_c/\sqrt{\Delta gd}$ and relative roughness $N = d/h$ shown in Figure 3, where h is the boundary
70 layer depth (or water level in wide channels). The reported relation appears to be valid over
71 6 decades of N with F_{dc} exhibiting at least 1.5 decades of variations. Another outcome
72 in Figure 3 is the presence of 3 regimes featuring approximate scaling laws of the form
73 $F_{dc} \sim N^{-\alpha}$: An $\alpha = 1/2$ for the so-called mini-roughness regime $N \in [10^{-6}, 10^{-4}]$, an
74 $\alpha = 1/6$ for the small-roughness regime $N \in [10^{-4}, 0.1]$, and $\alpha = 0$ for the large-roughness
75 regime $N \in [0.1, 1]$.
76

77 Instead of using separate arguments to explain each α value, it is shown here that a
78 single $F_{dc} - N$ curve can be recovered from a co-spectral budget (CSB) model that tracks
79 the effects of all eddies on τ_b . The proposed model is driven by the shape of the vertical
80 velocity spectrum $E_{ww}(k)$ instead of the turbulent kinetic energy spectrum $E_{tke}(k)$. That
81 $E_{ww}(k)$ explains the $F_{dc} - N$ is to be expected in vertical momentum transfer studies of wall-
82 stress. Moreover, the work here shows that the presence of an inverse cascade is not necessary
83 provided some steepening of the $E_{ww}(k)$ above and beyond its inertial scaling occurs at small

84 scales. However, links between local variables in the roughness sublayer above the bed and
 85 bulk variables must be revised to account for roughness effects as discussed elsewhere [34].
 86 The main theoretical novelties offered here are new perspectives about the curve featured
 87 in Figure 3, the transition zones between the various roughness scaling regimes, and the
 88 links between exponents α and the entire shape of $E_{ww}(k)$ that is characterized by multiple
 89 exponents. It also offers a pragmatic approach (i.e. a single expression) to modeling incipient
 90 motion within large-scale hydrodynamic models of sediment motion when U_c is to be used.

91 II. THEORY

92 A. Review of the Analysis by Ali-Dey

93 The insightful analysis by Ali and Dey [3, 26] to explain the three piece-wise scaling laws
 94 in Figure 3 is reviewed. At the point of incipient sediment motion (i.e. $U = U_c$) and from
 95 the aforementioned definitions, it directly follows that F_{dc} can be linked to θ_c using

$$96 \quad F_{dc} = \frac{U_c}{\sqrt{\Delta g d}} = \frac{u_*}{\sqrt{\Delta g d}} \frac{U_c}{u_*} = \sqrt{\theta_c} \frac{U_c}{u_*}. \quad (2)$$

97 When $Re^* > 400$ (i.e. fully rough flow regime), the Shields diagram in Figure 2 suggests
 98 that θ_c approaches a constant value independent of Re_* and F_{dc} is determined entirely from
 99 U_c/u_* . The aforementioned studies by Ali and Dey [3, 26] assumed that the flow is fully
 100 rough and θ_c is constant for differing N ranges. It was further assumed that $u_*^2 = v_l U_c$, where
 101 v_l is a characteristic turbulent vertical velocity [35] whereas horizontal velocity turbulent
 102 excursions scale with U_c . To determine v_l , a phenomenological model was then used given
 103 as [3, 26, 36]

$$104 \quad v_l \sim \left(\int_{l^{-1}}^{\infty} E_{tke}(k) dk \right)^{1/2}, \quad (3)$$

105 where l is a characteristic length scale of the eddy near the roughness bed assumed propor-
 106 tional to d [3, 26]. The $E_{tke}(k)$ is modeled with a single exponent so that $E_{tke}(k) \propto k^\sigma$.
 107 Based on dimensional analysis alone, Ali and Dey [3, 26] argued that $E_{tke}(k)$ must be related
 108 to bulk variables (U_c, h) only, and k so that

$$109 \quad \frac{E_{tke}(k)}{U_c^2 h} = A_e (kh)^\sigma. \quad (4)$$

110 In principle, $E_{tke}(k)$ must be formulated in the same plane (i.e. roughness sublayer) where
 111 τ_c is acting (see Figure 1). This co-location means that the scaling in equation 4 may be

112 plausible when local variables in this plane are linked to bulk variables without any roughness
 113 modifications. Inclusion of roughness effects may be possible if the similarity constant A_e in
 114 equation 4 is made to vary with a roughness length that depends on d . However, the work of
 115 Ali and Dey was focused on links between σ and α and ignored this revision. Accepting their
 116 arguments leading to equation 4, substituting equation 4 into equation 3, and integrating
 117 leads to

$$118 \quad \frac{v_l}{U_c} \sim \left(\frac{d}{h}\right)^{-(1+\sigma)/2}. \quad (5)$$

119 With this estimate of v_l , the turbulent shear stress τ_c can be computed from

$$120 \quad \tau_c = \rho u_*^2 \sim \rho v_l U_c \sim \rho U_c^2 \left(\frac{d}{h}\right)^{-(1+\sigma)/2}. \quad (6)$$

121 Inserting equation 6 into equation 2, the densimetric Froude number can now be derived as
 122 [3],

$$123 \quad F_{dc} \sim \sqrt{\theta_c} \left(\frac{d}{h}\right)^{(1+\sigma)/4} = \sqrt{\theta_c} (N)^{(1+\sigma)/4}. \quad (7)$$

124 That is, $\alpha = -(1 + \sigma)/4$. This completes the sought link between the scaling laws in
 125 the $F_{dc} - N$ curve shown in Figure 3 and exponents describing the decay of $E_{tke}(k)$ with
 126 decreasing eddy sizes. The three scaling regimes in the $F_{dc} - N$ diagram can be piece-wise
 127 recovered when assuming differing energy transfer mechanisms dominate the $E_{tke}(k)$.

- 128 1. When $\sigma = -5/3$, which is the scaling law expected for the inertial subrange for locally
 129 homogeneous and isotropic turbulence, an $\alpha = 1/6$ is recovered.
- 130 2. When $\sigma = -1$, which is the scaling law linked to attached eddies impinging on the
 131 surface [37–40], $\alpha = 0$ is recovered.
- 132 3. When $\sigma = -3$, an $\alpha = 1/2$ is recovered. Ali and Dey argued that such a scaling
 133 law in $E_{tke}(k)$ may be associated with a quasi-2D turbulence occurring over a smooth
 134 surface (i.e. small N) experiencing an inverse cascade in energy (or forward cascade in
 135 enstrophy). While not explicitly discussed by Ali and Dey, it has been shown elsewhere
 136 that the energy spectrum due to the presence of the enstrophy cascade leads to a new
 137 prediction for the so-called friction factor $f \propto (u_*/U_c)^2$ in rough pipes. This scaling
 138 law is $f \sim N^{+1}$ at very high Reynolds number [41]. Naturally, such a friction factor
 139 prediction results in $F_{dc} \sim N^{-1/2}$. For 3-D turbulence at very high Reynolds number,
 140 $f \sim N^{1/3}$ (Strickler scaling) again consistent with $\alpha = -1/6$.

141 To recap, the analysis by Ali and Dey makes use of two assumptions: (i) a scaling argu-
 142 ment between bulk and local flow variables just above the sediment bed that is independent
 143 of the roughness elements (e.g. A_e in equation 4) and (ii) a turbulent vertical velocity trans-
 144 porting momentum to the bed with its energy linked to its size by the turbulent kinetic
 145 energy spectrum $E_{tke}(k) \propto k^\sigma$. Last, to recover the $\alpha = 1/2$, the flow above the surface
 146 covered with sediments was assumed to be 2-D with an inverse cascade. It is to be pointed
 147 out that turbulent flows even above smooth-walls are inherently three-dimensional and are
 148 dominated by a forward energy cascade thereby prompting interest in alternative explana-
 149 tions to the reported $F_{dc} - N$ scaling relations, especially at small N . The co-spectral budget
 150 (CSB) model is now used to explore such alternative.

151 B. The Co-spectral Budget Model

152 Accepting the experimental results in Figure 3, we ask whether a single equation can
 153 be derived that recovers the entire $F_{dc} - N$ relations across all N assuming a constant θ_c
 154 and a generic shape for the energy spectrum. To answer this question, a phenomenological
 155 approach is to be followed that is based on the co-spectral budget (CSB) model. The CSB has
 156 been used to describe flow statistics in wide-ranging applications in stratified atmospheric
 157 flows, pipe-flow, and open channel flows [34, 37, 42–47]. In the CSB model, the turbulent
 158 shear stress within the roughness sublayer above the bed is linked to the co-spectrum using

$$159 \quad \tau_t = \tau_b = \rho_f \overline{u'w'} = \rho_f \int_0^\infty F_{uw}(k) dk, \quad (8)$$

160 where τ_t is the turbulent shear stress or the momentum flux, u' and w' are the turbulent
 161 velocity fluctuations in longitudinal (along x) and vertical (along z) directions, respectively,
 162 the over-line indicates averaging over coordinates of statistical homogeneity, and $F_{uw}(k)$
 163 is the co-spectrum. The co-spectral budget model must be formulated in the roughness
 164 sublayer at some $z = r$ shown in Figure 1 and is given by,

$$165 \quad \frac{\partial F_{uw}(k)}{\partial t} = P_{uw}(k) + T_{uw}(k) + \pi(k) - D_{uw}(k), \quad (9)$$

166 with

$$167 \quad P_{uw}(k) = \Gamma(z)E_{ww}(k); D_{uw}(k) = 2\nu k^2 F_{uw}(k), \quad (10)$$

168 where r is the thickness of the roughness sublayer assumed to be proportional to d , $P_{uw}(k)$ is
 169 a production term responsible for generating correlations between u' and w' at wavenumber k

170 due to the presence of a finite mean velocity gradient $\Gamma(z) = du/dz$ at height $z = r$ where the
 171 CSB is being formulated, $E_{ww}(k)$ is the vertical velocity energy spectrum at $z = r$, $T_{uw}(k)$ is
 172 the momentum flux transfer term across scales, $\pi(k)$ is a pressure-velocity decorrelation term
 173 often modeled using return to isotropy principles thereby reducing the correlation strength
 174 between u' and w' at scale k , $D_{uw}(k)$ is a viscous destruction term also responsible for
 175 decorrelating w' from u' . The $D_{uw}(k)$ is only significant at scales where the action of fluid
 176 viscosity is appreciable, which is determined by the Kolmogorov microscale $\eta = (\nu^3/\epsilon)^{1/4}$,
 177 where ϵ is the mean turbulent kinetic energy dissipation rate at $z = r$. Adopting the Rotta
 178 closure model for the return-to-isotropy but modified to include the isotropization of the
 179 production term [34, 42, 43, 47] yields

$$180 \quad \pi(k) = -C_R \frac{1}{t_r(k)} F_{uw}(k) - C_I \Gamma(z) E_{ww}(k), \quad (11)$$

181 where $C_R \approx 1.8$, $C_I = 3/5$ are the Rotta and isotropization of production constants [48, 49],
 182 and $t_r(k)$ is a wavenumber dependent relaxation time scale reflecting the time it takes for
 183 local isotropy to be attained for eddies of size $1/k$. When ignoring $D_{uw}(k)$ with respect
 184 to $\pi(k)$ for steady state conditions at high Reynolds number, this CSB model reduces to
 185 $P_{uw}(k) = \pi(k)$ allowing the determination of the co-spectrum at k

$$186 \quad F_{uw}(k) = \frac{1 - C_I}{C_R} \Gamma(z) E_{ww}(k) t_r(k), \quad (12)$$

187 where a plausible model for $t_r(k) = (k^3 E_{ww}(k))^{-1/2}$ [50, 51] is used. This $t_r(k)$ model recovers
 188 $\epsilon^{-1/3} k^{-2/3}$ in the so-called inertial subrange when $E_{ww}(k) \propto k^{-5/3}$. The co-spectrum can be
 189 integrated across all turbulent scales k to yield the shear stress acting on the bed given by

$$190 \quad u_*^2 = \frac{\tau_t}{\rho_f} = \frac{1 - C_I}{C_R} \Gamma(z) \int_0^\infty \frac{[E_{ww}(k)]^{1/2}}{k^{3/2}} dk. \quad (13)$$

191 To evaluate the turbulent stress, only the $E_{ww}(k)$ shape above the roughness elements within
 192 the roughness sublayer is now required. A schematic of $E_{ww}(k)$ consistent in shape with lab-
 193 oratory and field studies [52–54] is employed and summarized in Figure 4. Figure 4 presents
 194 the main regimes governing the shape of $E_{ww}(k)$: (i) A flat-portion presumably due to the
 195 randomizing effects of the boundary on the large-eddies, (ii) an inertial subrange regime
 196 characterized by a '-5/3' scaling, and (iii) a wall-damping regime labeled for convenience
 197 as the 'p-scale'. In prior studies where the CSB budget was formulated far from a bound-
 198 ary, a simplified flat to '-5/3' spectrum appeared sufficient at a given height z [37, 43, 44].

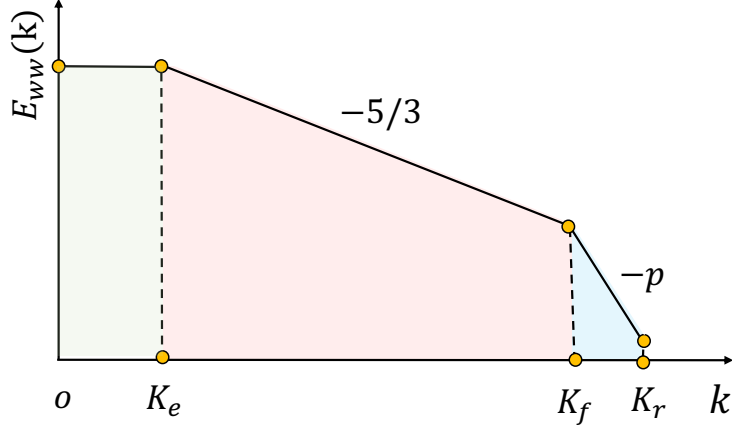


FIG. 4. Schematic of the vertical velocity energy spectrum $E_{ww}(k)$ as a function of wavenumber k in double-log representation. The right-tail effect is represented with a generic power-law exponent p . The K_e , K_f and K_r are characteristic wavenumbers delineating different energy production and transfer regimes in the vertical velocity. To solve the CSB model without depth-integration, the K_e , K_f and K_r must be linked to boundary conditions on the flow (i.e. h , and d).

200 However, for the large-roughness case where the CSB model is formulated in the rough-
 201 ness sublayer with respect to bulk variables, the tail-effects or 'p-scale' become significant
 202 and offer a link to d . This tail-effect has been reported in both field and laboratory ex-
 203 periments [53, 55, 56] near porous boundaries, where a slope ($p > 5/3$) has been observed
 204 above forests and gravel beds alike and even within rod canopies [56]. The aforementioned
 205 spectral regimes describing $E_{ww}(k)$ are associated with the following sizes: The flat portion
 206 applies to scales larger than $c_1 h (= 1/K_e)$, where $c_1 = 0.8$ is adopted based on pipe-flow ex-
 207 periments discussed elsewhere [43], the inertial scaling or '-5/3' applies to a range of scales
 208 bounded by $[K_e, K_f]$, where $K_f < K_r$, $c_2 r (= 1/K_r)$ and r is, as before, the thickness of
 209 the roughness sublayer assumed to be proportional to d with a proportionality constant of
 210 order unity. Many laboratory and field experiments on the roughness height [57, 58] show
 211 that the value of $c_2 \in [2, 5]$. Here, an intermediate value of $c_2 = 3.5$ is employed. The
 212 p scaling applies in the range of eddy sizes bounded by $[K_f, K_r]$. Since there is no clear
 213 formula available to specify K_f , an ad-hoc geometric averaging between h and r is adopted,
 214 i.e. $K_f = 1/(c_3 h^a r^{1-a})$ where a and c_3 are proportionality coefficients to be determined.
 215 Geometric averaging has been proposed for the atmospheric boundary layer when the need
 216 arises to determine an intermediate length scale bounded by very large and very small val-

217 ues impacting the flow [54]. For the inertial subrange spectrum, $E_{kol}(k) = C_k \epsilon^{2/3} k^{-5/3}$ is
 218 assumed, where $C_k = (24/55)C_k^1$ is the Kolmogorov constant for the vertical velocity and
 219 $C_k^1 = 1.5$ [49]. Energy is cascaded from the energy containing range to inertial subrange
 220 and is finally released as heat in the dissipation region not explicitly modeled here as the
 221 d is assumed to be larger than the Kolmogorov microscale. The $E_{ww}(k)$ drops off rapidly
 222 in the viscous dissipation regime so that the overall distortions to the turbulent stress is
 223 rather minor when ignored as discussed elsewhere [34]. This assumption is valid only when
 224 expressing the CSB model sufficiently high above the roughness elements while maintaining
 225 a high Reynolds number so that $r/\eta \gg 1$, where η is, as before, the Kolmogorov length
 226 scale. In the regime where eddies are commensurate in size to r , the continuity of $E_{ww}(k)$
 227 across scales requires that the p -regime varies as $E_p(k) = C_p \epsilon^{2/3} K_e^{p-5/3} k^{-p}$, where C_p is a
 228 proportionality coefficient dependent on p determined as $C_p = c_7 C_k c_3^{5/3-p} c_1^{p-5/3}$. Here, c_7 is
 229 a similarity coefficient that is connected to p as discussed elsewhere [56]. For an arbitrary p ,
 230 there is no clear theoretical basis to determine a priori c_7 . Hence, to constrain the resulting
 231 equation and minimize the degrees of freedom in the derivation here, one set of data from
 232 Lischtvan and Lebediev was selected and used to compute an optimal $c_7 (= 8)$. This c_7 value
 233 is used for the remaining data sets and sensitivity analyses on p . Moreover, this regime is
 234 expected to be significant when the roughness size r is large or the flow is shallow implying
 235 the magnitude of K_r is close to K_e . To summarize, the $E_{ww}(k)$ proposed here is allowed
 236 to vary with both h and d and experience multiple scaling exponents for differing k . This
 237 marks a point-of-departure from the $E_{tke}(k)$ in equation 4 assumed in the derivation of Ali
 238 and Dey.

239 With these eddy-size limits and their connections to the boundary conditions on the flow
 240 (h and d),

$$241 \quad u_*^2 = \frac{\tau_t}{\rho_f} = \frac{1 - C_I}{C_R} \Gamma(z) \int_{K_e}^{K_r} E_{ww}^{1/2}(k) k^{-3/2} dk. \quad (14)$$

242 Adopting the spectral shape in Figure 4 for $E_{ww}(k)$ results in

$$243 \quad u_*^2 = \zeta \left[C_p^{1/2} K_e^{3p-5} \int_{K_f}^{K_r} k^{-\frac{p+3}{2}} dk + C_k^{1/2} \int_{K_e}^{K_f} k^{-7/3} dk \right]; \\
 244 \quad \zeta = \frac{1 - C_I}{C_R} \Gamma(z) \epsilon(z)^{1/3}. \quad (15)$$

245 In principle, equation 15 requires a depth-integration to arrive at an expression linking U
 246 to u_* . As discussed in Bonetti *et al.* [34], analytical tractability becomes difficult and only a

247 numerical solution is possible. However, an intermediate approach may be taken if ζ , which
 248 is defined by local variables (Γ, ϵ) at $z = r$, can be related to bulk variables (U, h) using naive
 249 scaling arguments. Such intermediate approach bypasses the need for numerical integration
 250 and maintains the desired tractability here. It was argued by Gioia and Bombardelli [35]
 251 that at $z = r$

$$252 \quad \Gamma = \frac{du}{dz} = c_4 \frac{U}{r}; \epsilon = \frac{(c_5 U)^3}{h}. \quad (16)$$

253 These relations are hereafter labeled as GB02 and they have been used by Ali and Dey [3]
 254 when connecting the α in Figure 3 to σ through the dimensionless $E_{tke}(k)$. Both c_4 and
 255 c_5 were originally assumed constants independent of r in GB02, which cannot be realistic.
 256 To illustrate why, consider two pipes with identical diameters carrying the same flow rates
 257 (or U) but different surface roughness - one pipe is smooth while the other is fully rough.
 258 A scaling of the form $\epsilon = (c_5 U)^3 / D$ would yield the same bulk or local ϵ for these two
 259 pipes unless c_5 includes the roughness effects. To account for such effects, it was assumed
 260 elsewhere [34] that the product $c_4 c_5 = c_6 (r/h)^\beta$. When $\beta = 0$, the arguments by GB02 can
 261 be recovered and this limit may be expected for the range covered by the Strickler scaling
 262 ($N > 0.01$). We set β to be unity and $c_6 = 0.01$ for $N < 0.01$ and gradually transition to
 263 $\beta = 0$ as $N > 0.01$ guided by numerical results from the CSB model reported elsewhere
 264 [34] for rough surfaces where the 'virtual Nikuradse' equation holds. However, a separate
 265 sensitivity to the choice of β is also presented. Inserting these amended GB02 arguments
 266 into the CSB model for $\beta = 1$, equation 14 can be simplified to:

$$267 \quad \frac{\tau_t}{\rho_f U^2} = D_1 - D_2 N^{\frac{4}{3}(1-a)} + D_3 N^{\frac{p+1}{2}(1-a)} - D_4 N^{\frac{p+1}{2}}, \quad (17)$$

268 where D_i are coefficients given as:

$$269 \quad D_1 = \frac{3(1 - C_I)C_k^{1/2}}{4C_R} c_6 c_1^{4/3}; \quad D_2 = \frac{3(1 - C_I)C_k^{1/2}}{4C_R} c_6 c_3^{4/3}$$

$$270 \quad D_3 = \frac{2(1 - C_I)}{C_R} \frac{C_p^{1/2}}{p+1} c_6 c_1^{\frac{5-3p}{6}} c_3^{\frac{p+1}{2}}; \quad D_4 = \frac{2(1 - C_I)}{C_R} \frac{C_p^{1/2}}{p+1} c_6 c_1^{\frac{5-3p}{6}} c_2^{\frac{p+1}{2}}. \quad (18)$$

271 The c_3 is a coefficient determined by a and r/h , and C_p is determined by the 'p-scale' regime,
 272 D_1 and D_4 are determined according to empirical coefficients in prior discussion. Hence,
 273 only two degrees of freedom (a and c_3) are required to estimate D_2 and D_3 for a preset p .
 274 At the critical state when the sediment particles are entrained and upon assuming $r \approx d$,

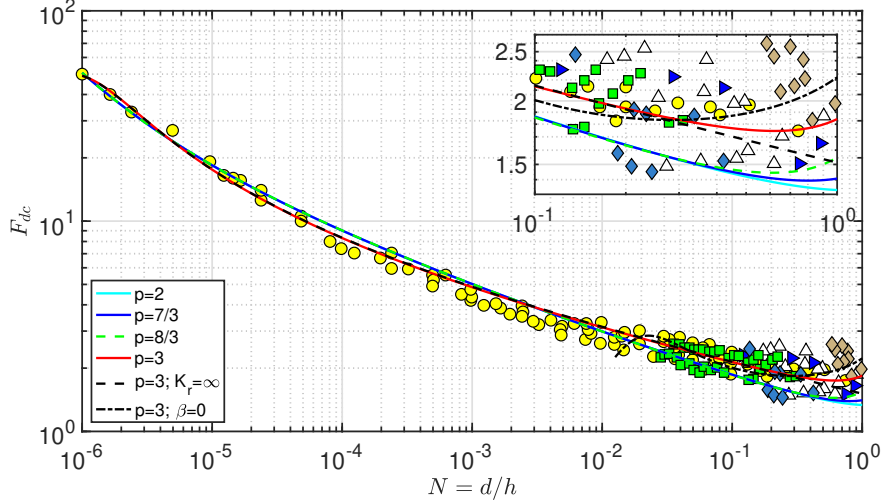


FIG. 5. Fitting the $F_{dc} - N$ derived from the CSB model to the data in Figure 3. The inset is an enlarged frame associated with the large-roughness regime ($N > 0.1$).

equations 2 and 17 can now be combined to yield a single curve given as

$$\frac{1}{F_{dc}^2} = D_{c1} - D_{c2}N^{\frac{4}{3}(1-a)} + D_{c3}N^{\frac{p+1}{2}(1-a)} - D_{c4}N^{\frac{p+1}{2}}, \quad (19)$$

where $D_{ci} = D_i/\theta_c$ are coefficients involving the Shields number and are assumed to be constant ($\theta_c = 0.06$) at high Re_* as shown in Figure 2. This is the sought result as it shows how the regimes in the $F_c - N$ are directly linked to the assumed shape of the vertical velocity spectrum. The links between the vertical velocity spectrum and the bulk flow variables are explicitly derived from GB02 subject to some amendments to include roughness effects.

III. RESULTS

For comparison, different values for p are set including the $p = 3$ employed by Dey and Ali [12]. Also, intermediate values (larger than the '5/3' scaling) of $p = 2, 7/3$ and $8/3$ are also shown to illustrate the dependence of α on p . For each p value, the CSB model is fitted to the measurements using nonlinear regression and the agreement is shown in Figure 5. The corresponding coefficients arising from the data fitting (for each p) are listed in Table III.

Figure 5 suggests that the CSB model can describe the reported measurements by Ali and Dey [3] reasonably. When $p = 3$, which is the value associated with the inverse cascade (or wakes generated by von Karman streets as discussed elsewhere [59]), a 'rebound' zone

TABLE I. Values of the relevant coefficients obtained by fitting the CSB model to the $F_{dc} - N$ data in Figure 3 assuming $c_1 = 0.8$, $c_2 = 3.5$, $c_6 = 0.01$, and $c_7 = 8$.

β	p	D_{c1}	$1 - a$	c_3	C_p	D_{c2}	D_{c3}	D_{c4}
1	2	0.02	0.21	18.81	0.68	1.35	2.07	0.17
1	7/3	0.02	0.20	10.06	0.96	0.59	1.32	0.23
1	8/3	0.02	0.19	6.76	1.45	0.34	1.08	0.32
1	3	0.02	0.11	8.58	0.22	0.47	0.90	0.15
1	3	0.02	0.11	8.53	0.22	0.47	0.89	none
0	3	0.02	0.37	7.60	0.25	0.40	0.74	0.15

is identified for $N \in [0.1, 1]$. Similarly, when $p > 5/3$, similar rebounds are also predicted by the CSB model. In fact, any value (e.g. $5/3$ to 3) for p will generate a rebound in this zone. This rebound implies that when k is closed to K_r , any deviations from the classic $5/3$ scaling in the vertical velocity spectrum influences the link between N and densimetric Froude number. However, the shape of the $F_{dc} - N$ curve for $N \in [10^{-6}, 0.1]$ appears insensitive to the precise choice of p . For this reason, a sensitivity analysis is conducted by reporting the Pearson linear correlation coefficients for a , c_3 , C_p and p as shown in Figure 6. The Pearson coefficient measures the strength of linear association between two variables and is bounded between -1 and $+1$. The analysis shows that the fitted coefficient a is sensitive to the choice of p as expected, since the Pearson correlation between a and p is close to 1 . The magnitude of the correlation between c_3 and p is also large according to Figure 6. This finding implies that the length scale $1/K_f$ is closely related to the choice of 'p-scale', which is expected. As p increases, the spectrum decays faster indicating the 'p-scale' influences the amount of energy in the vertical velocity spectrum above $1/K_f$. The formulation here suggests that the area under the spectrum governed by the $-5/3$ inertial scaling shrinks with K_f shifting closer to K_e and a becomes larger.

Table III shows that K_e contributes more to the intermediate wavenumber K_f than K_r since a is larger than $(1 - a)$. The analysis here identifies D_{c3} to be the dominant term, which suggests that the tail-effects cannot be entirely neglected when linking F_{dc} to N . However, the F_{dc} in the range of $N \in [10^{-6}, 0.1]$ appears robust to p variations when all terms are considered. Moreover, when K_r is extended to $+\infty$, which is shown in the black dashed

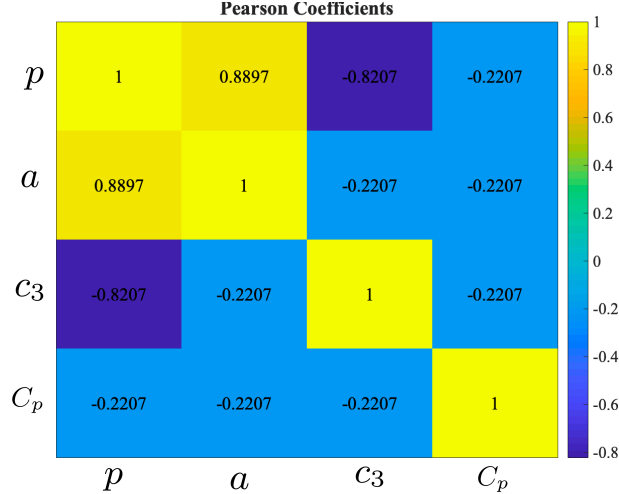


FIG. 6. Pearson correlation coefficients among a , c_3 and C_p corresponding to a given p . For example, the Pearson coefficient of two random variables (X, Y) is calculated as the covariance, $\text{cov}(X, Y)$ normalized by the standard deviations of the individual variables $(=\sigma_X, \sigma_Y)$, i.e., $\text{cov}(X, Y)/(\sigma_X\sigma_Y)$. The figure shows strong correlations between p and a , and between p and c_3 .

314 line, the rebound is no longer observed. This finding indicates that the spectral distortion
 315 in the vicinity of 5/3-law play an important role in large-scale roughness (i.e. $N > 0.1$),
 316 but not across all N values. According to GB02, β approaches zero for $N \in [10^{-2}, 1]$ to be
 317 consistent with the Stickler scaling for this range of N . If such scaling is adopted and $\beta = 0$
 318 in equation 19 throughout, then

$$319 \quad \frac{1}{F_{dc}^2} = D_{c1}N^{-1} - D_{c2}N^{\frac{1}{3}(1-4a)} + D_{c3}N^{\frac{p}{2}(1-a) - \frac{1}{2}(1+a)} - D_{c4}N^{\frac{p-1}{2}} \quad (20)$$

320 By setting $p = 3$, the modeled result from equation 20 is also shown in Figure 5. For
 321 $N \in [10^{-2}, 1]$, equation 20 also captures the data reported by Ali and Dey [3] where a
 322 rebound does not appear. However, for $N \in [10^{-6}, 10^{-2}]$, equation 20 fails to reproduce the
 323 entire $F_{dc} - N$ relation, which confirms that GB02 scaling arguments cannot be applied in
 324 the range $N \in [10^{-6}, 10^{-2}]$ without modifications.

325 IV. CAUTIONARY COMMENTS AND MODEL LIMITATIONS

326 The CSB model proposed here by no means offers finality to explaining the $F_{dc} - N$
 327 diagram reported by Ali and Dey [3], and its limitations are briefly reviewed. Before delving
 328 into the model limitations, a number of cautionary comments are warranted about the

329 processes being represented by the data in Ali and Dey [3]. To begin with, the connection
 330 between U_c and sediment incipient motion across many experiments may not be as universal
 331 as implied by Figure 3. For example, other data sources and studies [60] contradict the entire
 332 concept of critical velocity used by Ali and Dey [3]. A number of laboratory measurements
 333 also suggest no unique threshold velocity appears to be linked to sediment movement [61].
 334 The Reynolds number range over which θ_c is experimentally independent of Re_* must be
 335 viewed with caution. In flume experiments with water ($\nu = 1 \times 10^{-6} \text{ m}^2 \text{ s}^{-1}$), $u_* = (ghS_o)^{1/2}$,
 336 typical $h = 1\text{m}$ and $S_o = 0.01$ lead to an estimate of $u_* = 0.3\text{ms}^{-1}$ as a typical friction
 337 velocity. To maintain $Re_* > 400$ requires a minimum $d = 400\nu/u_* \approx 1 \times 10^{-3}\text{m}$. Hence, a
 338 minimum $N = d/h = 1 \times 10^{-3}$ can be experimentally maintained without θ_c being dependent
 339 on Re_* . This estimate is orders of magnitude larger than the $N \in [10^{-6}, 10^{-4}]$ reported in
 340 Ali and Dey [3] describing the scaling relation $F_{dc} \propto N^{-1/2}$. The finding here implies that
 341 the $F_{dc} - N$ scaling at the finest $N \in [10^{-6}, 10^{-4}]$ cannot be experimentally accessed for a θ_c
 342 strictly independent of Re_* using water (or air) as fluids in typical flumes (or wind tunnels).
 343 A θ_c that varies linearly with Re_*^{-1} (expected for $Re_* \ll 1$) may lead to an adjustment of
 344 the $F_{dc} - N$ relation by a factor that scales as $d^{-3/4}N^{1/4}$ both in the Ali-Dey and the CSB
 345 analysis. For $Re_* \in [3, 400]$, the situation may be subtler. The θ_c varies from a minimum of
 346 0.02 to a maximum of 0.06, but the variations in $(\theta_c)^{1/2}$ are between 0.14 and 0.24, which is
 347 much smaller than the factor of 10 variations in F_{dc} for $N \in [10^{-6}, 10^{-4}]$. So pragmatically,
 348 a near constant $(\theta_c)^{1/2}$ may still be acceptable even in the range of $N \in [10^{-6}, 10^{-4}]$, perhaps
 349 explaining the robustness of the $\alpha = 1/2$ for this range of N in typical flume experiments.

350 From a theoretical perspective, the space-time distribution of eddies on and within the
 351 bed are needed and formal double-averaging must be used to obtain upscaled approximations
 352 starting from single-particle equations and its interaction with neighboring particles. The
 353 CSB model proposed here makes no such attempt and it must be viewed only as a comple-
 354 mentary explanation to the insightful but piece-wise analysis offered by Ali and Dey [3]. The
 355 CSB model only accounted for two-terms: a stress production and pressure-decorrelation.
 356 Transfer of stresses across scales as well as molecular effects are ignored (though they can be
 357 incorporated in principle). Moreover, the CSB model assumed that the time for the return
 358 to isotropy at any scale can be inferred from the vertical velocity energy content, which may
 359 not be a valid approximation (relaxation time and time to isotropy can differ for differing k
 360 regimes). Perhaps among the most ad-hoc assumptions made in the CSB model derivation

361 are links between local and bulk variables. While the links employed here accommodate
 362 expected deviations from those proposed by GB02 and used by Ali and Dey [3], they remain
 363 questionable across the entire range of roughness values. Another ad-hoc assumption are the
 364 links between the transition zones across scales in the assumed vertical velocity spectrum
 365 and the variables h and d . To assess how robust the findings here are to these assumed links,
 366 a sensitivity analysis was conducted. This analysis identified the zones where assumptions
 367 about the p -scale impacted the entire $F_{dc} - N$ curve.

368 Despite all the aforementioned criticisms, it is safe to state that the work here provides
 369 a single expression that summarizes the data featured by Ali and Dey [3]. The theoretical
 370 argument leading to this single expression may be viewed as naive but pragmatic. Thus,
 371 the expression derived here may be imminently used in models aimed at describing sedi-
 372 ment transport across large spatial domains, a topic that is gaining prominence given the
 373 advancement in remote sensing platforms.

374 V. CONCLUSION

375 The multi-scaling regimes of sediment entrainment encoded in the $F_{dc} - N$ curve reported
 376 by Ali and Dey [3] have been considered using a co-spectral budget model where integration
 377 across all turbulent scales and z are needed. A new single expression that links F_{dc} to N
 378 was proposed using the CSB model that recovers all 6 decades of N variations. The CSB
 379 model shows that the vertical velocity spectrum $E_{ww}(k)$ can explain the entire $F_{dc} - N$ curve,
 380 not just piece-wise scaling. Moreover, the k^{-3} scaling used by Ali and Dey, a signature of
 381 an enstrophy cascade dominating the spectrum, is not necessary per se. The CSB model
 382 highlights another issue rarely considered when linking spectral exponents to scaling laws
 383 in the $F_{dc} - N$ curve: Inferring local variables from bulk variables. This inference is by
 384 no means straight-forward, especially for N values that fall outside the original Strickler
 385 N regime. Studies using the so-called virtual Nikuradse [34, 62] as well as studies dealing
 386 with intermittency corrections to turbulent spectra [63, 64] all point to deviations from the
 387 Strickler scaling for $N \in [10^{-6}, 10^{-2.5}]$. These effects were partly accommodated for through
 388 a non-zero β here.

389 While the CSB model can describe quantitatively the measured $F_{dc} - N$ curve, its 3 key
 390 parameters a , c_3 , and C_p cannot be predicted on theoretical grounds. To be able to predict

391 these coefficients requires models that describe the shape of the vertical velocity spectrum
392 (including any transition zones) only as a function of d , h , and U , a topic that is better kept
393 for future research.

394 ACKNOWLEDGMENTS

395 The authors thank A. Packman for the many constructive comments and helpful sugges-
396 tions on an earlier version of this manuscript. G.K. acknowledges support from the U.S.
397 National Science Foundation (NSF-AGS-1644382 and NSF-IOS-1754893).

-
- 398 [1] CT Yang, “Incipient motion and sediment transport,” *Journal of the Hydraulics Division* **99**,
399 1679–1704 (1973).
- 400 [2] PY Julien, *Erosion and sedimentation* (Cambridge University Press, New York, 2010) pp.
401 112–126.
- 402 [3] S Ali and S Dey, “Origin of the scaling laws of sediment transport,” *Proceedings of the Royal*
403 *Society A* **473**, 20160785 (2017).
- 404 [4] GK Gilbert, *U.S. Geological Survey Professional Paper*, Tech. Rep. issn:2330-7102 (1914).
- 405 [5] MC Miller, IN McCave, and P.D Komar, “Threshold of sediment motion under unidirectional
406 currents,” *Sedimentology* **24**, 507–527 (1977).
- 407 [6] Z Jiang and PK Haff, “Multiparticle simulation methods applied to the micromechanics of
408 bed load transport,” *Water Resources Research* **29**, 399–412 (1993).
- 409 [7] AG Hunt, “A probabilistic treatment of fluvial entrainment of cohesionless particles,” *Journal*
410 *of Geophysical Research: Solid Earth* **104**, 15409–15413 (1999).
- 411 [8] I McEwan, M Sørensen, J Heald, S Tait, G Cunningham, D Goring, and B Willetts, “Prob-
412 abilistic modeling of bed-load composition,” *Journal of Hydraulic Engineering* **130**, 129–139
413 (2004).
- 414 [9] Al Shields, “Anwendung der aehnlichkeitsmechanik und der turbulenzforschung auf die
415 geschiebebewegung,” PhD Thesis Technical University Berlin (1936).
- 416 [10] AB Shvidchenko, G Pender, and TB Hoey, “Critical shear stress for incipient motion of
417 sand/gravel streambeds,” *Water Resources Research* **37**, 2273–2283 (2001).

- 418 [11] Z Cao, G Pender, and J Meng, “Explicit formulation of the Shields diagram for incipient
419 motion of sediment,” *Journal of Hydraulic Engineering* **132**, 1097–1099 (2006).
- 420 [12] S Dey and S Ali, “Advances in modeling of bed particle entrainment sheared by turbulent
421 flow,” *Physics of Fluids* **30**, 061301 (2018).
- 422 [13] JM Buffington and DR Montgomery, “A systematic analysis of eight decades of incipient
423 motion studies, with special reference to gravel-bedded rivers,” *Water Resources Research* **33**,
424 1993–2029 (1997).
- 425 [14] MH García, EM Laursen, C Michel, and JM Buffington, “The legend of AF Shields,” *Journal*
426 *of Hydraulic Engineering* **126**, 718–723 (2000).
- 427 [15] S Dey and A Papanicolaou, “Sediment threshold under stream flow: A state-of-the-art review,”
428 *KSCE Journal of Civil Engineering* **12**, 45–60 (2008).
- 429 [16] PR Wilcock, “Critical shear stress of natural sediments,” *Journal of Hydraulic Engineering*
430 **119**, 491–505 (1993).
- 431 [17] AE Lobkovsky, B Jensen, A Kudrolli, and DH Rothman, “Threshold phenomena in ero-
432 sion driven by subsurface flow,” *Journal of Geophysical Research: Earth Surface* **109** (2004),
433 10.1029/2004JF000172.
- 434 [18] M Church and MA Hassan, “Mobility of bed material in Harris Creek,” *Water Resources*
435 *Research* **38**, 1–12 (2002).
- 436 [19] M Righetti and C Lucarelli, “May the Shields theory be extended to cohesive and
437 adhesive benthic sediments?” *Journal of Geophysical Research: Oceans* **112** (2007),
438 10.1029/2006JC003669.
- 439 [20] G Parker, PR Wilcock, C Paola, WE Dietrich, and J Pitlick, “Physical basis for quasi-
440 universal relations describing bankfull hydraulic geometry of single-thread gravel bed rivers,”
441 *Journal of Geophysical Research: Earth Surface* **112** (2007), 10.1029/2006JF000549.
- 442 [21] C Parker, NJ Clifford, and CR Thorne, “Understanding the influence of slope on the threshold
443 of coarse grain motion: Revisiting critical stream power,” *Geomorphology* **126**, 51–65 (2011).
- 444 [22] PL Wiberg and JD Smith, “Calculations of the critical shear stress for motion of uniform and
445 heterogeneous sediments,” *Water Resources Research* **23**, 1471–1480 (1987).
- 446 [23] PD Komar, “Comparisons of the hydraulics of water flows in Martian outflow channels with
447 flows of similar scale on Earth,” *Icarus* **37**, 156–181 (1979).

- 448 [24] JF Kok, “An improved parameterization of wind-blown sand flux on Mars that includes the
449 effect of hysteresis,” *Geophysical Research Letters* **37** (2010), 10.1029/2010GL043646.
- 450 [25] DM Burr, JP Emery, RD Lorenz, GC Collins, and PA Carling, “Sediment transport by liquid
451 surficial flow: Application to Titan,” *Icarus* **181**, 235–242 (2006).
- 452 [26] S Ali and S Dey, “Impact of phenomenological theory of turbulence on pragmatic approach
453 to fluvial hydraulics,” *Physics of Fluids* **30**, 045105 (2018).
- 454 [27] LL Lischtvan and VV Lebediev, “Gidrologia i gidraulika v mostovom doroshnom, straitielvie,”
455 *Hydrology and Hydraulics in Bridge and Road Building*, Gidrometeoizdat, Leningrad (1959).
- 456 [28] CR Neill, “Mean-velocity criterion for scour of coarse uniform bed-material,” In Proceedings of
457 the 12th Congress of International Association for Hydraulic Research, Fort Collins, Colorado,
458 USA **3**, 46–54 (1967).
- 459 [29] K Ashida and M Bayazit, “Initiation of motion and roughness of flows in steep channels,”
460 In Proceedings of the 15th Congress of International Association for Hydraulic Research,
461 Istanbul, Turkey **1**, 475–484 (1973).
- 462 [30] ML Olivero, “Movimiento incipiente de partículas en flujo torrencial,” Special Report: Uni-
463 versity of Los Andes, Meridad, Venezuela , 169 (1984).
- 464 [31] J Aguirre-Pe and R Fuentes, “Movement of big particles in steep, macro-rough streams,” In
465 Proceedings of the 24th Congress of International Association for Hydraulic Research, Madrid,
466 Spain **A**, 149–158 (1991).
- 467 [32] JC Bathurst, WH Graf, and HH Cao, “Initiation of sediment transport in steep channels with
468 coarse bed material, paper presented at Euromech 156: Mechanics of Sediment Transport,”
469 In *Mechanics of Sediment Transport* (eds BM Summer, A Muller) , 207–213 (1982).
- 470 [33] JC Bathurst, HH Cao, and WH Graf, “The data from the EPFL study of hydraulics and
471 sediment transport in a steep flume,” Report no. CH-1015. Ecole Polytechnique Fédérale de
472 Lausanne (EPFL) Lausanne, Switzerland **64** (1984).
- 473 [34] S Bonetti, G Manoli, C Manes, A Porporato, and G Katul, “Mannings formula and Stricklers
474 scaling explained by a co-spectral budget model,” *Journal of Fluid Mechanics* **812**, 1189–1212
475 (2017).
- 476 [35] G Gioia and FA Bombardelli, “Scaling and similarity in rough channel flows,” *Physical Review*
477 *Letters* **88**, 014501 (2002).

- 478 [36] G Gioia, N Guttenberg, N Goldenfeld, and P Chakraborty, “Spectral theory of the turbulent
479 mean-velocity profile,” *Physical Review Letters* **105**, 184501 (2010).
- 480 [37] T Banerjee and G Katul, “Logarithmic scaling in the longitudinal velocity variance explained
481 by a spectral budget,” *Physics of Fluids* **25**, 125106 (2013).
- 482 [38] P Drobinski, P Carlotti, JL Redelsperger, V Masson, RM Banta, and RK Newsom, “Numerical
483 and experimental investigation of the neutral atmospheric surface layer,” *Journal of the
484 Atmospheric Sciences* **64**, 137–156 (2007).
- 485 [39] G Katul and CR Chu, “A theoretical and experimental investigation of energy-containing
486 scales in the dynamic sublayer of boundary-layer flows,” *Boundary-Layer Meteorology* **86**,
487 279–312 (1998).
- 488 [40] G Katul, A Porporato, and V Nikora, “Existence of k^{-1} power-law scaling in the equilibrium
489 regions of wall-bounded turbulence explained by Heisenberg’s eddy viscosity,” *Physical Review
490 E* **86**, 066311 (2012).
- 491 [41] N Guttenberg and N Goldenfeld, “Friction factor of two-dimensional rough-boundary turbu-
492 lent soap film flows,” *Physical Review E* **79**, 065306 (2009).
- 493 [42] G Katul, A Porporato, C Manes, and C Meneveau, “Co-spectrum and mean velocity in
494 turbulent boundary layers,” *Physics of Fluids* **25**, 091702 (2013).
- 495 [43] G Katul and C Manes, “Cospectral budget of turbulence explains the bulk properties of
496 smooth pipe flow,” *Physical Review E* **90**, 063008 (2014).
- 497 [44] G Katul, A Porporato, S Shah, and E Bou-Zeid, “Two phenomenological constants explain
498 similarity laws in stably stratified turbulence,” *Physical Review E* **89**, 023007 (2014).
- 499 [45] G Katul, D Li, H Liu, and S Assouline, “Deviations from unity of the ratio of the turbulent
500 Schmidt to Prandtl numbers in stratified atmospheric flows over water surfaces,” *Physical
501 Review Fluids* **1**, 034401 (2016).
- 502 [46] D Li, G Katul, and S Zilitinkevich, “Closure schemes for stably stratified atmospheric flows
503 without turbulence cutoff,” *Journal of the Atmospheric Sciences* **73**, 4817–4832 (2016).
- 504 [47] KA McColl, G Katul, P Gentine, and D Entekhabi, “Mean-velocity profile of smooth channel
505 flow explained by a cospectral budget model with wall-blockage,” *Physics of Fluids* **28**, 035107
506 (2016).
- 507 [48] BE Launder, G Reece, and W Rodi, “Progress in the development of a Reynolds-stress
508 turbulence closure,” *Journal of Fluid Mechanics* **68**, 537–566 (1975).

- 509 [49] SB Pope, *Turbulent Flows* (Cambridge University Press, Cambridge, U.K., 2000) p. 754.
- 510 [50] GK Vallis, *Atmospheric and Oceanic Fluid Dynamics* (Cambridge University Press, Cam-
511 bridge, U.K., 2017) p. 936.
- 512 [51] D Li and G Katul, “On the linkage between the $k^{-5/3}$ spectral and $k^{-7/3}$ cospectral scaling
513 in high-Reynolds number turbulent boundary layers,” *Physics of Fluids* **29**, 065108 (2017).
- 514 [52] GJ Kunkel and I Marusic, “Study of the near-wall-turbulent region of the high-Reynolds-
515 number boundary layer using an atmospheric flow,” *Journal of Fluid Mechanics* **548**, 375–402
516 (2006).
- 517 [53] C Manes, D Poggi, and L Ridolfi, “Turbulent boundary layers over permeable walls: scaling
518 and near-wall structure,” *Journal of Fluid Mechanics* **687**, 141–170 (2011).
- 519 [54] KG McNaughton, RJ Clement, and JB Moncrieff, “Scaling properties of velocity and tem-
520 perature spectra above the surface friction layer in a convective atmospheric boundary layer,”
521 *Nonlinear Processes in Geophysics* **14**, 257–271 (2007).
- 522 [55] D Cava and G Katul, “Spectral short-circuiting and wake production within the canopy trunk
523 space of an alpine hardwood forest,” *Boundary-Layer Meteorology* **126**, 415–431 (2008).
- 524 [56] D Poggi and G Katul, “Two-dimensional scalar spectra in the deeper layers of a dense and
525 uniform model canopy,” *Boundary-Layer Meteorology* **121**, 267–281 (2006).
- 526 [57] RD Hey, “Flow resistance in gravel-bed rivers,” *Journal of the Hydraulics Division* **105**, 365–
527 379 (1979).
- 528 [58] LC Van Rijn, “Sediment transport, Part iii: bed forms and alluvial roughness,” *Journal of*
529 *Hydraulic Engineering* **110**, 1733–1754 (1984).
- 530 [59] D Poggi, G Katul, and B Vidakovic, “The role of wake production on the scaling laws of
531 scalar concentration fluctuation spectra inside dense canopies,” *Boundary-Layer Meteorology*
532 **139**, 83–95 (2011).
- 533 [60] JW Lavelle and HO Mofjeld, “Do critical stresses for incipient motion and erosion really
534 exist?” *Journal of Hydraulic Engineering* **113**, 370–385 (1987).
- 535 [61] T Pächtz and O Durán, “The cessation threshold of nonsuspended sediment transport across
536 aeolian and fluvial environments,” *Journal of Geophysical Research: Earth Surface* **123**, 1638–
537 1666 (2018).
- 538 [62] BH Yang and DD Joseph, “Virtual Nikuradse,” *Journal of Turbulence* **10**, 1–28 (2009).

- 539 [63] N Goldenfeld and G Gioia, “Roughness-induced criticality in turbulence,” Physical Review
540 Letters **96**, 044503 (2006).
- 541 [64] M Mehrafarin and N Pourtolami, “Intermittency and rough-pipe turbulence,” Physical Review
542 E **77**, 055304 (2008).